

Theoretical investigation of the signal-to-noise ratio in fluorescence lifetime imaging

Johan Philip

Department of Mathematics, The Royal Institute of Technology, SE-100 44 Stockholm, Sweden

Kjell Carlsson

Biomedical and X-Ray Physics, The Royal Institute of Technology, Stockholm Center for Physics, Astronomy and Biotechnology, SE-106 91 Stockholm, Sweden

Received May 28, 2002; revised manuscript received September 18, 2002; accepted September 23, 2002

We deduce the signal-to-noise ratio for fluorescence lifetime imaging when using frequency-domain methods. We assume mono-exponential decay and quantum-noise-limited performance. The results are compared with Monte Carlo simulations with good agreement. We also compare our results with previous investigations of time-domain methods for fluorescence lifetime imaging. For a given number of detected photons, we find that frequency-domain and time-domain methods are equally good. The correct choice of detection technique and its parameters is important for obtaining good results. © 2003 Optical Society of America

OCIS codes: 000.5490, 170.1790, 170.2520, 170.3650, 270.5290.

1. INTRODUCTION

In the fluorescence process, a molecule absorbs a photon and, after a certain delay, emits a photon of (generally) longer wavelength. Typically, both the absorbed and emitted photons are in the visible spectrum, but ultraviolet and infrared wavelengths are also possible. Molecules displaying this behavior (fluorophores) are usually rather complex organic chemicals. When the fluorescence process is repeated, the time delay between the absorption and the emission of a photon varies statistically for a fluorophore molecule. The average time delay is called the fluorescence lifetime, denoted by τ . If a large number of fluorophore molecules are illuminated by a short pulse of light (Dirac pulse) at time $t = 0$, the intensity of the emitted fluorescence will vary according to

$$I(t) = I_0 \exp(-t/\tau), \quad t \geq 0. \quad (1)$$

Biomedical preparations are often labeled with fluorescent substances before microscopical study. In this way, specific labeling of interesting parts can be made. The intensity of the fluorescent light is usually studied, and images are often recorded by photography or CCD image sensors. Also, laser-scanning methods are used for recording images of the fluorescence distribution in both two and three dimensions. In addition to fluorescence intensity imaging, it has recently become popular to record fluorescence lifetime images. In a fluorescence lifetime image, the pixel values do not represent light intensity but rather represent fluorescence lifetime τ .^{1–9} Such images can be useful tools in the biomedical field.^{10–18} This trend has been stimulated by the development of probes with lifetimes that are sensitive to, e.g., Ca^{2+} concentration or pH.^{19,20}

Compared with light intensity measurements, fluorescence lifetime has the advantage of a reduced sensitivity to errors caused by light absorption, scattering, and

photobleaching. A number of different techniques can be used for measuring fluorescence lifetime, many of which have been in use for a long time. These methods can be divided into two main groups: time-domain methods and frequency-domain methods. In time-domain methods, the fluorescence light intensity decay is measured after excitation with a short pulse of light.¹⁵ In frequency-domain methods, the fluorescent sample is illuminated with light whose intensity varies periodically in time. The fluorescent light will also display periodic intensity variations at the same frequency, and the phase angle or the degree of modulation of the fluorescent light is measured.²¹ From these measurements, the lifetime can be calculated.

In many cases where fluorescence lifetime imaging is used, the number of recorded photons per pixel is relatively small. This is the case especially in confocal microscopy. In such cases, there can be a considerable uncertainty in the recorded values due to photon quantum noise. Also, other sources of noise will influence the results, but these are often of minor importance. The obvious remedy is to collect more photons, but this often leads to photobleaching, excessive recording times, and blurred images due to specimen movement. It is therefore important to record the available photons as efficiently as possible, and to process the resulting signals in the best possible way, so that losses in signal-to-noise ratio (SNR) can be kept to a minimum.

The number of photons recorded during a fixed measuring period is Poisson distributed. Denote the parameter of the distribution by N . This means that the number of photons has mean N and standard deviation \sqrt{N} . The SNR of the process is $N/\sqrt{N} = \sqrt{N}$. This is the ultimate SNR that we can get with this number of detected photons. When fluorescence lifetime imaging is performed, multiple intensity measurements must be combined, a

process that often reduces the SNR. To quantify the performance of a lifetime imaging technique, we will use the *F*-value introduced by Draaijer *et al.*¹³ The *F*-value is defined as $F = \sqrt{N}\sigma_\tau/\tau$, where σ_τ is the standard deviation in repeated measurements of the lifetime value τ . Technically, the *F*-value can be described as "normalized relative rms noise," where the normalization is relative to an ideal intensity measurement with the same number of detected photons (i.e., $\text{SNR} = \sqrt{N}$, yielding an *F*-value of unity). In all lifetime measurements, we have $F \geq 1$; and the closer the value to unity, the better the performance.

The SNR for time-domain fluorescence lifetime measurements has been investigated previously. Time-correlated single-photon counting (TCSPC)²² has been investigated by Köllner and Wolfrum.²³ In this technique, the measured fluorescence intensity decay function is fitted to (in the simplest case) a mono-exponential function. With the use of TCSPC, *F*-values arbitrarily close to unity can be obtained provided that a sufficient time resolution (number of recording channels) and total measurement time are used. This means that TCSPC has the potential to utilize the available photons as efficiently as is physically possible. In reality, both the total measurement time and the number of channels must be limited. However, it takes only eight channels to reach an *F*-value of approximately 1.1.

Time gating can be considered a simplified version of TCSPC, where, in the simplest case, only two measurement channels (time windows) are used. After pulse excitation, the integrated fluorescence light intensities in two consecutive time windows are measured. From the ratio of these intensities, the lifetime can easily be calculated. The performance of this technique has been investigated both theoretically and by Monte Carlo methods by Ballew and Demas.²⁴ In the case of two time windows of equal width, the best *F*-value, 1.5, is obtained for a window width of 2.5τ . As expected, better performance can be obtained with more than two windows.⁹

Both TCSPC and time gating require short pulses of light (in the picosecond or femtosecond regime). Although longer pulses can in principle be used, this requires compensation that will compromise the performance. By using frequency-domain, rather than time-domain, methods, one can drop the requirement for short pulses. In this case, the fluorophore is illuminated by light whose intensity varies periodically in time. The traditional frequency-domain method uses sinusoidally intensity-modulated excitation with a frequency that is usually in the range from ten up to a few hundred megahertz. The sine modulation is transferred to the fluorescent light, though weakened and phase shifted. By measuring the phase shift or the degree of modulation, one can calculate the lifetime of the fluorescence process.²¹ Although frequency-domain methods have been used for a long time,²⁵ rather little has been published concerning their SNR performance and how they can be optimized. Draaijer *et al.*¹³ have made computer simulations, assuming detection by an image intensifier and excitation either by a sinusoid or a train of Dirac pulses. It was found that the best (i.e., lowest) *F*-values attainable for these two cases are 6 and 1.5, respectively. The optimum param-

eter settings were not reported. In another study by Carlsson and Liljeborg,²⁶ it was theoretically shown that, when lock-in detection is used, an *F*-value of 3.7 could be obtained for sine-modulated excitation. The optimum modulation frequency was found to be $0.1/\tau$ in this case. We felt that a more thorough and systematic investigation of the performance and the optimization of frequency-domain methods was needed. Therefore we have undertaken a theoretical study to assess what *F*-values are obtainable and how the experimental parameters should be chosen to achieve these values. In addition to the theoretical investigations, we have also performed Monte Carlo simulations to get an independent verification of the theoretical results. We recently presented some preliminary results, mainly Monte Carlo simulations, from this study in a summarized form.²⁷ In this paper, we will develop the full mathematical theory for different frequency-domain imaging methods and present the optimum working parameters.

We consider three measuring techniques:

1. Phase measurements using lock-in detection. In this method, a detector transforms the emitted fluorescence light into an electric output signal that is fed to two lock-in amplifiers. In each of these amplifiers, the signal is multiplied by a sinusoid and low-pass filtered. The sinusoids have the same frequency as that of the illumination, and their phase angles can be adjusted by the operator.²⁸ The values of the two output signals from the lock-in amplifiers are recorded and used to estimate the lifetime τ of the fluorescent light.

2. Phase measurements using an image intensifier. In this case, the fluorescent light is amplified, and the amplification factor is sine modulated at the same frequency as that of the illumination. The average light intensity, after amplification, is recorded for different phase angles of the sine-modulated amplification factor, and these values are used for estimating the lifetime.

3. Demodulation measurements, which are made with either an image intensifier or lock-in amplifiers. In this case, the lifetime is obtained from the degree of modulation of the fluorescence signal compared with that of the excitation.

The results presented are not restricted to the imaging case but are valid for fluorescence lifetime measurements in general. While an image intensifier is likely to be used only for imaging purposes, lock-in detection of a detector signal can be used in nonimaging applications. Our results are applicable also to such measurements. In non-imaging situations, the lifetime value is usually based on many more detected photons, so that the SNR is higher and parameter optimization is less important.

2. THEORY

A. Accuracy Estimation

Our estimates of τ will be of the form $\bar{\tau} = u/v$, where u and v are estimates of random variables U and V . We must assume that V cannot take the value zero or even small values. To estimate the accuracy of τ , we write

$$\tau = \frac{U}{V} = \frac{\mu_1 + \sigma_1 Y_1}{\mu_2 + \sigma_2 Y_2}, \quad (2)$$

where μ_1 and μ_2 are the means, and σ_1 and σ_2 are the standard deviations, of U and V , respectively. The Y_i are random variables with mean = 0 and variance = 1. We introduce the notation $\kappa_1 = \sigma_1/\mu_1$ and $\kappa_2 = \sigma_2/\mu_2$, assume that $|\kappa_2|$ is (much) smaller than unity, and use series expansion:

$$\begin{aligned} \frac{U}{V} &= \frac{\mu_1}{\mu_2} \frac{1 + \kappa_1 Y_1}{1 + \kappa_2 Y_2} \\ &= \frac{\mu_1}{\mu_2} (1 + \kappa_1 Y_1 - \kappa_2 Y_2 - \kappa_1 \kappa_2 Y_1 Y_2 \\ &\quad + \kappa_2^2 Y_2^2 + \dots). \end{aligned} \quad (3)$$

We get the expectation of τ :

$$E\{\tau\} = \frac{\mu_1}{\mu_2} (1 - \rho \kappa_1 \kappa_2 + \kappa_2^2 + \dots), \quad (4)$$

where $\rho = E\{Y_1 Y_2\}$.

Squaring Eq. (3), taking expectations, and omitting moments of order > 2 , we get

$$E\{\tau^2\} = \left(\frac{\mu_1}{\mu_2}\right)^2 (1 + \kappa_1^2 + 3\kappa_2^2 - 4\rho\kappa_1\kappa_2). \quad (5)$$

Subtracting the square of $E\{\tau\}$, we get

$$\begin{aligned} \sigma_\tau^2 = D^2\{\tau\} &= \left(\frac{\mu_1}{\mu_2}\right)^2 (\kappa_1^2 + \kappa_2^2 - 2\rho\kappa_1\kappa_2 \\ &\quad - \rho^2 \kappa_1^2 \kappa_2^2 - \kappa_2^4 + 2\rho\kappa_1\kappa_2^3). \end{aligned} \quad (6)$$

Our estimates will be constructed such that $\mu_1/\mu_2 = \tau$. The F -value for the various methods will be based on the ratio σ_τ/τ (see Section 1).

B. Model

The fluorescence caused by illumination with a Dirac light pulse at time $t^* = 0$ is assumed to be $f(t^*) = f_0 \exp(-t^*/\tau^*)$, $t^* \geq 0$. It is the average fluorescence lifetime τ^* that shall be estimated. Here we have used the asterisk to denote time measured in seconds. In the following, we shall study a scaled problem and use a dimensionless time variable t and a dimensionless parameter τ . The period T of the illuminating light is used for the scaling. Define

$$t = \frac{2\pi}{T} t^*, \quad \tau = \frac{2\pi}{T} \tau^*.$$

The dimensionless time period will be 2π . It is good mathematical practice to work with dimensionless variables. The formulas become simpler. The time and frequency dependence of a calculated τ can be recovered by unscaling with the formula $\tau^* = (T/2\pi)\tau = \tau/\omega$, where ω is the angular frequency of the light modulation.

The fluorescence caused by a Dirac pulse at time $t = 0$ will be

$$f(t) = \frac{1}{\tau} \exp(-t/\tau), \quad t \geq 0, \quad (7)$$

which is normalized so that its integral value over the positive axis equals unity.

The illumination is assumed to be a periodic function $e(t)$, now with period 2π . With such an illumination, the intensity of the fluorescent light is the convolution $e * f$ of e and f , which also is a function with period 2π (Fig. 1).

The fluorescent light is so weak that it cannot be thought of as a continuous flow but shall be seen as a sequence of photons. The total number of photons in a measurement can be as low as 100 or fewer. The photon generation is assumed to be a random Poisson process with a parameter proportional to $e * f$. The probability that a photon shall be emitted in the short time interval $(t, t + \Delta t)$ is $\gamma(e * f)(t)\Delta t$, where γ is proportional to the average number of photons per period.

C. Lock-In Detection

If a photon is detected at time t , the first lock-in amplifier outputs the signal $\sin(t + \phi_1)$, where ϕ_1 is a parameter chosen by the operator. The sum s_1 of these signals over a measuring period is the data delivered from the measurement. The same applies to the second lock-in amplifier, but with the phase angle ϕ_2 . Being generated from the same random process, s_1 and s_2 are observations of dependent random variables.

1. Calculation of Mathematical Expectations for Illumination with a Train of Dirac Light Pulses

Let us consider the idealized case in which $e(t)$ is an infinite sequence of Dirac pulses of size unity in the points $t = 2\pi k$, k integer. We get the periodic convolution

$$p(t) = (e * f)(t) = \frac{\exp(-t/\tau)}{\tau[1 - \exp(-2\pi/\tau)]}, \quad 0 \leq t < 2\pi. \quad (8)$$

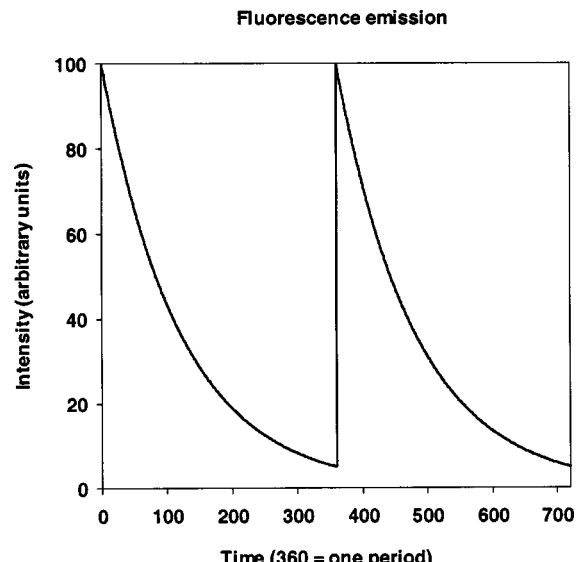


Fig. 1. Fluorescence light intensity as a function of time with excitation by a train of Dirac pulses.

The mathematical expectation with respect to the current probability density $p(t)dt$ is denoted by $E\{\cdot\}$. For any function $g(t)$, this means that

$$E\{g(t)\} = \int_0^{2\pi} g(t)p(t)dt. \quad (9)$$

We shall use Fourier series for handling the periodic functions and define the complex Fourier coefficients by

$$\begin{aligned} p_k &= \int_0^{2\pi} \exp(-ikt)p(t)dt \\ &= \frac{1}{1 + ik\tau}, \quad -\infty < k < \infty. \end{aligned} \quad (10)$$

Let the output per period from lock-in amplifier i be X_i , $i = 1, 2$. We get

$$\begin{aligned} E\{X_i\} &= \int_0^{2\pi} \sin(t + \phi_i)p(t)dt \\ &= \text{Im}\left\{ \int_0^{2\pi} \exp[i(t + \phi_i)]p(t)dt \right\} \\ &= \text{Im}[\exp(i\phi_i)p_{-1}] \\ &= \text{Im}\left(\frac{\cos\phi_i + i\sin\phi_i}{1 - i\tau} \right) \\ &= \frac{\tau\cos\phi_i + \sin\phi_i}{1 + \tau^2}. \end{aligned} \quad (11)$$

We get

$$\frac{E\{X_1\}}{E\{X_2\}} = \frac{\tau\cos\phi_1 + \sin\phi_1}{\tau\cos\phi_2 + \sin\phi_2}. \quad (12)$$

If the Dirac pulses have size γ instead of unity, the average number of photons in a measurement lasting n periods will be $n\gamma$. We shall denote this quantity by N . Using the observation s_i as an estimate of $NE\{X_i\}$, we get the following estimator of the sought τ .

$$\bar{\tau} = \frac{s_1\sin\phi_2 - s_2\sin\phi_1}{-s_1\cos\phi_2 + s_2\cos\phi_1}. \quad (13)$$

Let u and v be the numerator and the denominator of Eq. (13), so that $\bar{\tau} = u/v$. Denoting the corresponding random variables by U and V , we get

$$\begin{aligned} E\{U\} &= NE\{X_1\sin\phi_2 - X_2\sin\phi_1\} \\ &= NE\{\sin\phi_2\sin(t + \phi_1) - \sin\phi_1\sin(t + \phi_2)\} \\ &= N\sin(\phi_2 - \phi_1)E\{\sin t\}. \end{aligned} \quad (14)$$

Defining $\Delta\phi = \phi_2 - \phi_1$, we get

$$\begin{aligned} E\{U\} &= N\sin\Delta\phi E\{\sin t\} \\ &= N\sin\Delta\phi \text{Im}(p_{-1}) = N\sin\Delta\phi \frac{\tau}{1 + \tau^2}. \end{aligned} \quad (15)$$

In the same way,

$$\begin{aligned} E\{V\} &= N\sin\Delta\phi E\{\cos t\} \\ &= N\sin\Delta\phi \text{Re}(p_{-1}) \\ &= N\sin\Delta\phi \frac{1}{1 + \tau^2}. \end{aligned} \quad (16)$$

It follows that $E\{U\}/E\{V\} = \tau$, but this is not the same as $E\{\bar{\tau}\} = E\{U/V\}$.

To carry out the error analysis of Subsection 2.A, we will need the second moments of U and V . To this end, we need a closer discussion of the photon process. Divide each period of the time axis into, say, M intervals of length $\Delta t = 2\pi/M$, where M is large. For interval number k containing the point t_k , the probability that a photon is generated is $p(t_k)\Delta t$, and if that happens, the lock-in amplifier i will output $\sin(t_k + \phi_i)$. The expected contributions from this interval to U and U^2 are

$$\begin{aligned} \Delta U &= [\sin(t_k + \phi_1)\sin\phi_2 - \sin(t_k + \phi_2)\sin\phi_1]p(t_k)\Delta t \\ &\quad \times \sin\phi_1]p(t_k)\Delta t \\ &= \sin\Delta\phi \sin(t_k)p(t_k)\Delta t, \\ \Delta U^2 &= [\sin(t_k + \phi_1)\sin\phi_2 - \sin(t_k + \phi_2)\sin\phi_1]^2p(t_k)\Delta t \\ &= \sin^2\Delta\phi \sin^2(t_k)p(t_k)\Delta t. \end{aligned}$$

When summing the ΔU and letting $\Delta t \rightarrow 0$, we get the same integral as that in Eq. (15).

The contribution to the variance of U is $\Delta U^2 - (\Delta U)^2$ from each interval. The second term is of the order of $(\Delta t)^2$ and can be neglected. The contributions from disjoint intervals are independent. When summing them, we get

$$\begin{aligned} \sigma_1^2 &= E\{U^2\} = N\sin^2\Delta\phi E\{\sin^2 t\} \\ &= \frac{N}{2}\sin^2\Delta\phi E\{1 - \cos 2t\} \\ &= \frac{N}{2}\sin^2(\Delta\phi)[1 - \text{Re}(p_{-2})] \\ &= \frac{N}{2}\sin^2(\Delta\phi)\left(1 - \frac{1}{1 + 4\tau^2}\right), \end{aligned} \quad (17)$$

$$\begin{aligned} \sigma_2^2 &= E\{V^2\} = N\sin^2\Delta\phi E\{\cos^2 t\} \\ &= \frac{N}{2}\sin^2(\Delta\phi)\left(1 + \frac{1}{1 + 4\tau^2}\right), \end{aligned} \quad (18)$$

$$\begin{aligned} \rho\sigma_1\sigma_2 &= E\{UV\} = N\sin^2\Delta\phi E\{\sin t\cos t\} \\ &= \frac{N}{2}\sin^2\Delta\phi \text{Im}(p_{-2}) \\ &= N\sin^2(\Delta\phi) \frac{\tau}{1 + 4\tau^2}. \end{aligned} \quad (19)$$

Inserting Eqs. (15)–(19) in Eq. (4), we get

$$E\{\bar{\tau}\} = \tau\left[1 + \frac{2}{N} \frac{\tau^2(1 + \tau^2)^2}{1 + 4\tau^2} + \dots\right]. \quad (20)$$

Here N equals the expected number of photons in the measurement. From Eq. (6), we have

$$\sigma_\tau^2 = D^2\{\bar{\tau}\} = \frac{\tau^2(1 + \tau^2)^2(1 + 2\tau^2)}{N(1 + 4\tau^2)}. \quad (21)$$

The F -value will be

$$F = \frac{\sqrt{N}\sigma_\tau}{\tau} = (1 + \tau^2) \left(\frac{1 + 2\tau^2}{1 + 4\tau^2} \right)^{1/2}. \quad (22)$$

It is counterintuitive that F is independent of $\Delta\phi$, and one could believe that very small $\Delta\phi$ would give higher F . However, the Monte Carlo tests confirm that even $\Delta\phi = 0.1^\circ$ with $N = 240$ photons per measurement gives approximately the same F as does a bigger $\Delta\phi$. Generally, $\Delta\phi = 90^\circ$ is a natural choice. The frequency dependence of F can be recovered by replacing τ with $\omega\tau^*$ in Eq. (22), where τ^* is the fluorescence lifetime measured in seconds (Fig. 2). F is an increasing function of τ , so its minimum is attained for $\tau = 0$. For instance, $\tau^* = 3$ ns and $f < 27$ MHz give $F < 1.1$.

2. Square-Wave and “Gauss-Like” Pulse Excitation
Excitation by Dirac pulses is, of course, impossible to accomplish in practice. Also “near-Dirac” pulses often require expensive equipment. Therefore we shall consider excitation by broader pulses and start with square waves with duty cycle a . The fluorescence light intensity will be the convolution of the train of Dirac pulses e of Subsection 2.C.1, the decay function f , and the function h_a :

$$h_a(t) = \begin{cases} \frac{1}{2\pi a}, & |t| < a\pi \\ 0, & \text{else} \end{cases}. \quad (23)$$

The Fourier coefficients of the convolution are the products of the p_k and the Fourier coefficients of h_a . The products are

$$a_0 = 1, \quad a_k = \frac{\sin k\pi a}{k\pi a} \frac{1}{1 + ik\tau}, \quad k \neq 0. \quad (24)$$

To get an estimate of τ and its accuracy, we replace the p_k of Subsection 2.C.1 by the a_k . Since $h_a(t)$ is an even function, a real factor is introduced, but, otherwise, the formulas are the same. We get

$$E\{U\} = N \sin \Delta\phi \operatorname{Im}(a_{-1}) = N \sin(\Delta\phi) \frac{\sin \pi a}{\pi a} \frac{\tau}{1 + \tau^2}, \quad (25)$$

so formula (13) for $\bar{\tau}$ is still valid. For the variance, we have

$$\begin{aligned} E\{U^2\} &= \frac{N}{2} \sin^2(\Delta\phi) \left[1 - \operatorname{Re} \left(\frac{\sin 2\pi a}{2\pi a} \frac{1}{1 - i2\tau} \right) \right] \\ &= \frac{N}{2} \sin^2(\Delta\phi) \left(1 - \frac{\sin 2\pi a}{2\pi a} \frac{1}{1 + 4\tau^2} \right). \quad (26) \end{aligned}$$

The other expectations are obtained analogously. By inserting $\tau = \omega\tau^*$, we recover the frequency dependence. Figure 3 shows the F -value as a function of modulation frequency for square waves with different duty cycles a .

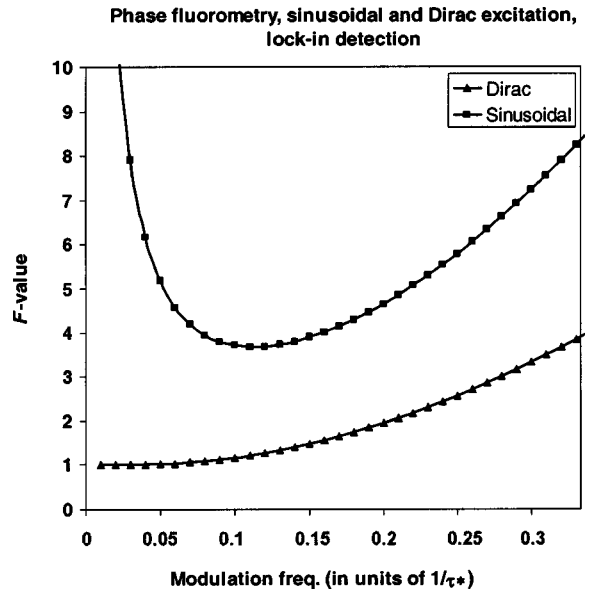


Fig. 2. Normalized relative rms noise F as a function of modulation frequency with lock-in detection. Low F -values represent good performance. Theoretically, $F \geq 1$. Curves shown are for excitation by a train of Dirac pulses and sinusoidal excitation.

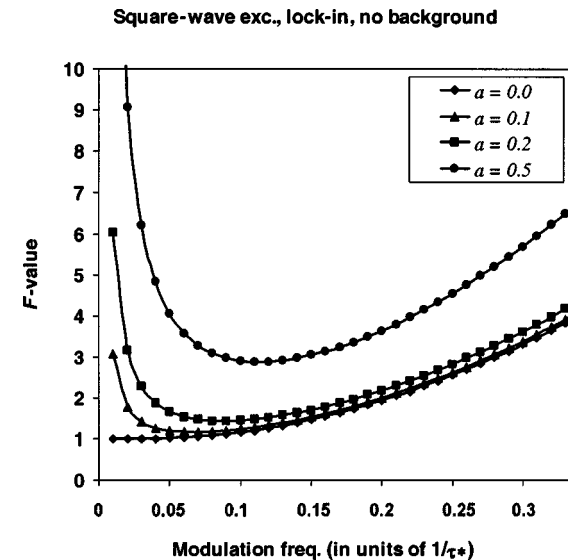


Fig. 3. F -value as a function of modulation frequency for square-wave excitation with different duty cycles a ($a = 0.0$ represents Dirac pulses).

The best results (i.e., lowest F -values) are obtained when a is small ($a = 0$ corresponds to a train of Dirac pulses). The best F -values obtainable for $a = 0.5$ and $a = 0.1$ are 2.9 and 1.2, respectively. The optimum modulation frequency also depends on a but is usually in the region $0.05/\tau^* - 0.1/\tau^*$.

When intensity-modulated light is generated by using, for example, an electro-optic modulator, it is often not possible to shut off the light completely. We may therefore have a background intensity ($=b$), implying that $h_a(t)$ in fact has the form

$$h_{ab}(t) = \frac{1}{2\pi[1 - (1-a)(1-b)]} \begin{cases} 1, & |t| < a\pi \\ b, & \text{else} \end{cases}. \quad (27)$$

Then the a_k are replaced by

$$b_k = \frac{a(1-b)}{1 - (1-a)(1-b)} \frac{\sin k\pi a}{k\pi a} \frac{1}{1 + ik\tau}, \quad k \neq 0, \quad (28)$$

and formula (13) for $\bar{\tau}$ is still valid. The factor $a(1-b)/[1 - (1-a)(1-b)]$ of b_{-2} will enter the expression for the variance of U [compare with Eq. (26)]. For duty cycles $a = 0.5$ and 0.1 and $b = 0.05$, the F -values will increase by 11% and 95%, respectively, compared with those for the case of no background (Fig. 4). The loss of performance caused by background is thus most pronounced at low duty cycles. At a background level of 5%, we can actually see that a duty cycle of 0.2 will give better performance than a duty cycle of 0.1 (Fig. 4). Compare with Fig. 3, showing the background-free case, where the order of the curves is reversed.

Because of bandwidth limitations, practical light modulators will not be able to generate perfect square-wave pulses, with or without background. Let us consider smoothed versions of the above-mentioned excitations. We will use the following "Gauss-like" smoothing kernel:

$$s_c(t) = \begin{cases} \frac{2c}{\pi} \cos^2 ct, & |t| < \frac{\pi}{2c} \\ 0, & \text{else} \end{cases}. \quad (29)$$

Usually, we use $c = 2$ so that the support of s_c is a quarter of a period, and its FWHM is half of that (Fig. 5). The Fourier coefficients of s_c are

$$c_0 = 1, \quad c_{\pm 2c} = \frac{1}{2},$$

Square-wave exc., lock-in, backgr. 0.05

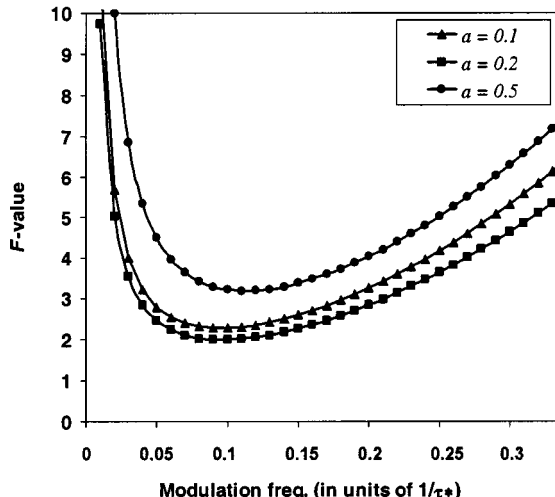


Fig. 4. Same as Fig. 3, but with a background light intensity of the excitation that is 5% of that of the peak value. Note that the order of the curves with $a = 0.1$ and $a = 0.2$ is reversed compared with those in Fig. 3.

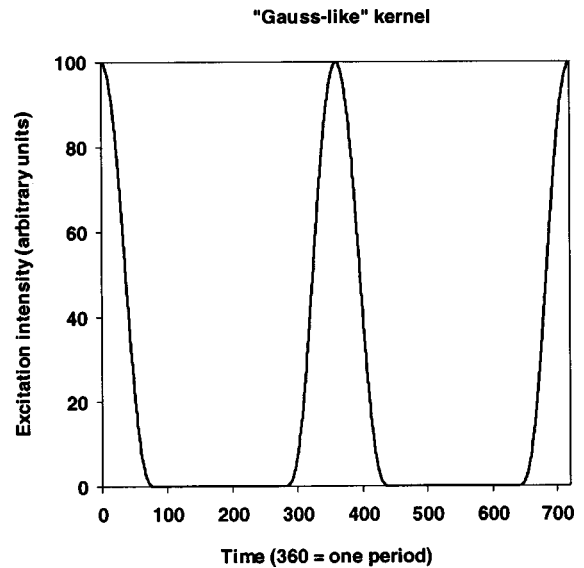


Fig. 5. Smooth "Gauss-like" kernel. The excitation intensity function was obtained by convolving a square wave with this smoothing kernel.

$$c_k = \frac{4c^2}{4c^2 - k^2} \frac{\sin(k\pi/2c)}{k\pi/2c}, \quad k \neq 0, \pm 2c. \quad (30)$$

With the excitation h_{ab} smoothed by s_c , the factor c_{-2} will also enter the expression (26) for the variance of U :

$$\begin{aligned} E\{U^2\} = & \frac{N}{2} \sin^2(\Delta\phi) \\ & \times \left[1 - \frac{4c^2}{4c^2 - 4} \frac{\sin(\pi/c)}{\pi/c} \frac{a(1-b)}{1 - (1-a)(1-b)} \right. \\ & \left. \times \frac{\sin 2\pi a}{2\pi a} \frac{1}{1 + 4\tau^2} \right]. \end{aligned} \quad (31)$$

With $a = 0.2$, $b = 0.0$, and $c = 2$, we get an F_{\min} -value that is 12% larger than that for the corresponding non-smoothed square waves (compare Figs. 3 and 6). Adding a background level b of 0.05 to the smooth excitation will have an effect similar to that observed for square-wave excitation. Thus the largest increase in F -value will be at low duty cycles. The results will resemble those shown in Fig. 4, but with 5%–10% higher F -values. Practically, this means that the loss in performance will be relatively small if a train of femtosecond illumination pulses is replaced by nanosecond pulses.

3. Sinusoidal Excitation

Excitation by sinusoidally intensity-modulated light is common and easy to produce. Then the illumination function will be

$$e(t) = \frac{1}{2\pi}(1 + m \sin t), \quad (32)$$

where m is the degree of modulation ($0 < m \leq 1$). The fluorescent light is the convolution g of e and f . We get

$$\begin{aligned}
2\pi q(t) &= 1 + \frac{m}{\tau} \int_0^\infty \sin(t-x) \exp(-x/\tau) dx \\
&= 1 + \frac{m}{\tau} \operatorname{Im} \left\{ \int_0^\infty \exp[i(t-x) - x/\tau] dx \right\} \\
&= 1 + \frac{m}{\tau} \operatorname{Im} \left[\exp(it) \frac{1}{i + 1/\tau} \right] \\
&= 1 + \frac{m}{1 + \tau^2} (\sin t - \tau \cos t). \tag{33}
\end{aligned}$$

Define $\alpha = \arctan \tau$, and let α replace τ as the sought parameter. Then we can write

$$q(t) = \frac{1}{2\pi} [1 + m \cos \alpha \sin(t - \alpha)]. \tag{34}$$

The only Fourier coefficients of this function that are different from zero are

$$\begin{aligned}
q_0 &= 1, & q_1 &= -\frac{i}{2} m \cos \alpha \exp(-i\alpha), \\
q_{-1} &= \frac{i}{2} m \cos \alpha \exp(i\alpha). \tag{35}
\end{aligned}$$

We get

$$E\{X_i\} = \operatorname{Im}\{\exp(i\phi_i)q_{-1}\} = \frac{m \cos \alpha}{2} \cos(\phi_i + \alpha) \tag{36}$$

and use the estimate

$$\frac{s_1}{s_2} = \frac{E\{X_1\}}{E\{X_2\}} = \frac{\cos(\phi_1 + \alpha)}{\cos(\phi_2 + \alpha)}. \tag{37}$$

Rearranging, we obtain

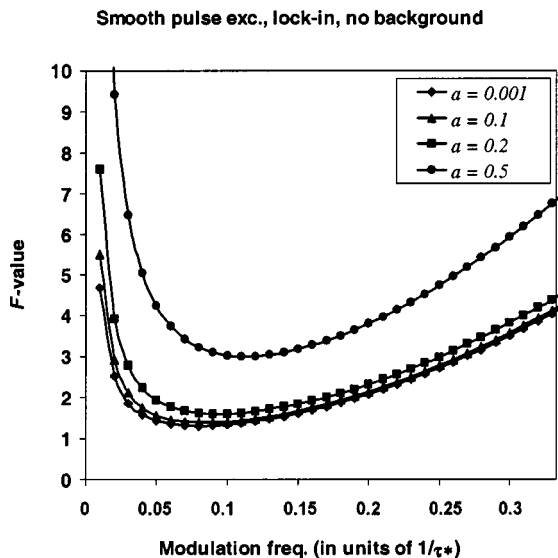


Fig. 6. F -value as a function of modulation frequency for excitation with Gauss-like pulses and lock-in detection. a represents the duty cycle for the square wave that was convolved with the smoothing kernel. Compare with Fig. 3.

$$\bar{\tau} = \tan \bar{\alpha} = \frac{s_1 \cos \phi_2 - s_2 \cos \phi_1}{s_1 \sin \phi_2 - s_2 \sin \phi_1}. \tag{38}$$

As above, we put $\bar{\tau} = u/v$, let N denote the total number of photons in a measurement, and get

$$\begin{aligned}
E\{U\} &= N\{\cos \phi_2 \operatorname{Im}[\exp(i\phi_1)q_{-1}] \\
&\quad - \cos \phi_1 \operatorname{Im}[\exp(i\phi_2)q_{-1}]\} \\
&= \frac{N}{2} m \cos \alpha \sin \Delta\phi \sin \alpha. \tag{39}
\end{aligned}$$

In the same way,

$$E\{V\} = \frac{N}{2} m \cos \alpha \sin \Delta\phi \cos \alpha. \tag{40}$$

We will also need

$$\begin{aligned}
E\{U^2\} &= N(\cos^2 \phi_2 E\{X_1^2\} + \cos^2 \phi_1 E\{X_2^2\} \\
&\quad - 2 \cos \phi_1 \cos \phi_2 E\{X_1 X_2\}). \tag{41}
\end{aligned}$$

Here

$$E\{X_i^2\} = \frac{1}{2} \operatorname{Re}[1 - \exp(i2\phi_i)q_{-2}] = \frac{1}{2}, \tag{42}$$

$$\begin{aligned}
E\{X_1 X_2\} &= \frac{1}{2} \operatorname{Re}\{\exp[i(\phi_1 - \phi_2)] \\
&\quad - \exp[i(\phi_1 + \phi_2)]q_{-2}\} \\
&= \frac{1}{2} \cos(\phi_1 - \phi_2). \tag{43}
\end{aligned}$$

Insertion in Eq. (41) gives the variance [compare with Eq. (17)]:

$$E\{U^2\} = E\{V^2\} = \frac{N}{2} \sin^2 \Delta\phi. \tag{44}$$

After some trigonometric manipulations, we find that $E\{UV\} = 0$. This gives $\kappa_1 = \sqrt{2/N}/(m \cos \alpha \sin \alpha)$, $\kappa_2 = \sqrt{2/N}/(m \cos \alpha \cos \alpha)$, and $\rho = 0$. From Eqs. (4) and (6), we get

$$E\{\bar{\tau}\} = \tau \left(1 + \frac{2}{Nm^2} \frac{1}{\cos^4 \alpha} \right), \tag{45}$$

$$\sigma_\tau = \tau \sqrt{\frac{2}{N} \frac{1}{m \cos^2 \alpha \sin \alpha}}, \tag{46}$$

giving

$$F = \frac{\sqrt{N}\sigma_\tau}{\tau} = \frac{\sqrt{2}}{m \cos^2 \alpha \sin \alpha} = \frac{\sqrt{2}(1 + \tau^2)^{3/2}}{m \tau}. \tag{47}$$

Note also that this F is independent of $\Delta\phi$, as in the pulse excitation case. The frequency dependence of F is recovered by inserting $\tau = \omega\tau^*$ in Eq. (47). Figure 2 shows the F -value as a function of the modulation frequency for $m = 1$. The best F -value, 3.7, is obtained for $\tau = \sqrt{0.5}$, corresponding to a frequency of $0.11/\tau^*$. In analogy with the case of square waves, we may have a background intensity level, so that the intensity never drops to zero. This means that $m < 1$, and the F -value will be higher by a factor of $1/m$.

D. Image Intensifier

In an image intensifier, the light amplification factor is varied with a local (phase-shifted) sinusoid. In this way, the incoming periodically varying light intensity is multiplied by the local sinusoid. The output signal s is the integral of the product. We assume that the amplification factor is $1 + \sin(t + \phi)$, so that it is nonnegative. [Compare with the factor $\sin(t + \phi)$ of the lock-in technique.] Two successive measurements are made with different phase angles ϕ_1 and ϕ_2 , so that s_1 and s_2 are obtained. Assuming as above that the total number of photons per measurement equals N , the two measurements will have the averages $E\{s_i\} = NE\{X_i\}$. A third measurement is made with no modulation in order to estimate the average intensity of the sample. The third observation s_3 will be Poisson distributed with $E\{s_3\} = N$ and $D^2\{s_3\} = N$. The situation differs from the lock-in case in which one incoming light intensity is transformed to an electric signal. This signal is fed into several mixers that use different phase angles. This makes the lock-in data dependent, while the image intensifier data are independent. With three output data, the image intensifier technique will need three times as many photons for a measurement as that for the lock-in technique. This has been taken into account when calculating the F -values.

1. Dirac Pulse Excitation

The excitation is the same as that in the lock-in case. With an image intensifier, we get [compare with Eq. (11)]

$$E\{X\} = 1 + \text{Im}[\exp(i\phi)p_{-1}] = 1 + \frac{\tau \cos \phi + \sin \phi}{1 + \tau^2}. \quad (48)$$

The following estimate is used [compare with Eq. (12)]:

$$\frac{s_1 - s_3}{s_2 - s_3} = \frac{\tau \cos \phi_1 + \sin \phi_1}{\tau \cos \phi_2 + \sin \phi_2}. \quad (49)$$

Rearranging, we obtain the estimator [compare with Eq. (13)]

$$\bar{\tau} = \frac{s_1 \sin \phi_2 - s_2 \sin \phi_1 - s_3(\sin \phi_2 - \sin \phi_1)}{-s_1 \cos \phi_2 + s_2 \cos \phi_1 + s_3(\cos \phi_2 - \cos \phi_1)}. \quad (50)$$

As above, we put $\bar{\tau} = u/v$. The expressions for $E\{U\}$ and $E\{V\}$ are the same as those in Eqs. (15) and (16). We get

$$D^2\{U\} = N[\sin^2 \phi_2 D^2\{X_1\} + \sin^2 \phi_1 D^2\{X_2\} + (\sin \phi_2 - \sin \phi_1)^2]. \quad (51)$$

We have

$$\begin{aligned} D^2\{X_i\} &= E\{X_i^2\} \\ &= 1 + 2 \text{Im}[\exp(i\phi_i)p_{-1}] \\ &\quad + \frac{1}{2} \text{Re}[1 - \exp(2i\phi_i)p_{-2}] \\ &= \frac{3}{2} + 2 \frac{\tau \cos \phi_i + \sin \phi_i}{1 + \tau^2} \\ &\quad - \frac{1}{2} \frac{\cos 2\phi_i - 2\tau \sin 2\phi_i}{1 + 4\tau^2}. \end{aligned} \quad (52)$$

Insertion of Eq. (52) in Eq. (51) will produce $D^2\{U\}$. Replacing the sines with cosines, we get $D^2\{V\}$. We also have

$$\begin{aligned} E\{UV\} &= -N[\sin \phi_2 \cos \phi_2 D^2\{X_1\} \\ &\quad + \sin \phi_1 \cos \phi_1 D^2\{X_2\} + (\cos \phi_2 - \cos \phi_1) \\ &\quad \times (\sin \phi_2 - \sin \phi_1)]. \end{aligned} \quad (53)$$

Contrary to the development in former sections, these averages and variances cannot be written as functions of $\Delta\phi = \phi_2 - \phi_1$. We have investigated how σ_r/τ varies with ϕ_1 and ϕ_2 and found a ratio of approximately 5 between the largest and smallest values. The reason for this angular dependence is illustrated in Fig. 7, which shows the distribution of Monte Carlo-simulated measurements in the u/v plane. The phase angles producing the lowest F -value depend on τ and are given in Fig. 8. The frequency dependence of F is recovered by replacing τ with $\omega\tau^*$ (Fig. 9). We get $F_{\min} = 2.1$, attained for $\tau = 0$.

2. Sinusoidal Excitation

The excitation is the same as that in the lock-in case. We get [compare with Eq. (36)]

$$E\{X\} = 1 + \text{Im}[\exp(i\phi)p_{-1}] = 1 + \frac{m \cos \alpha}{2} \cos(\phi + \alpha). \quad (54)$$

The following estimate is used [compare with Eq. (37)]:

$$\frac{s_1 - s_3}{s_2 - s_3} = \frac{\cos(\phi_1 + \alpha)}{\cos(\phi_2 + \alpha)}. \quad (55)$$

Rearranging, we obtain the estimate

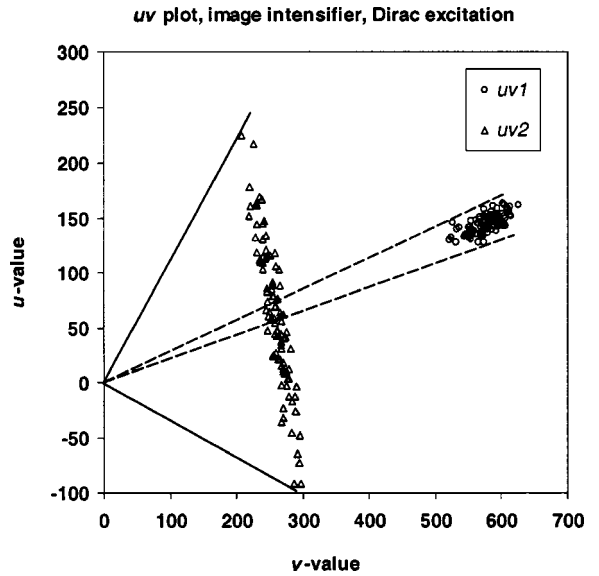


Fig. 7. Plot of u versus v from 100 Monte Carlo tests with Dirac excitation and image intensifier detection for $\tau = 0.25$ (frequency = $0.04/\tau^*$). The cluster $uv1$ to the right is for $\phi_1 = 230^\circ$ and $\phi_2 = 280^\circ$, and the vertical band $uv2$ is for $\phi_1 = 60^\circ$ and $\phi_2 = 260^\circ$. Since $\bar{\tau} = u/v$, the spread in the angles to the points gives the spread in $\bar{\tau}$. $uv1$ is obtained with the angles given in Fig. 8 below. $uv2$ is an unfortunate choice of ϕ_1 and ϕ_2 .

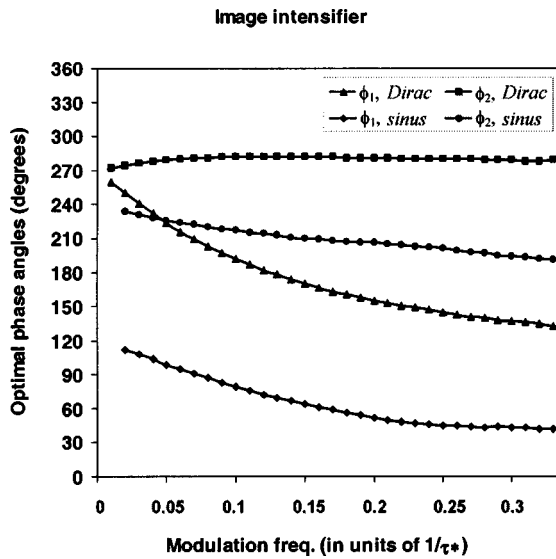


Fig. 8. Optimal phase angles for image intensifier detection as a function of modulation frequency. Both sinusoidal and Dirac pulse excitations are shown.

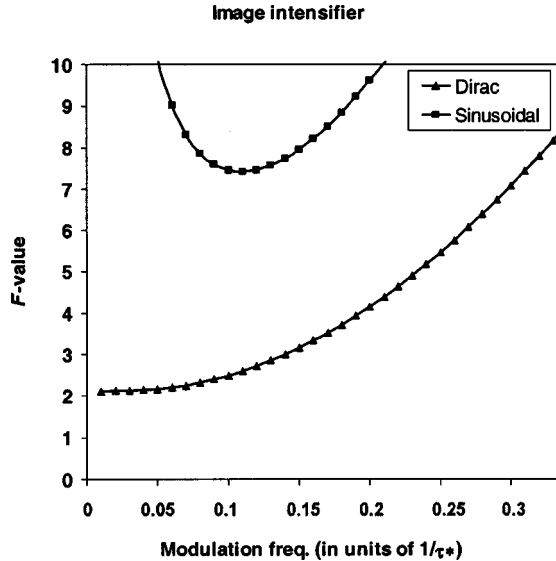


Fig. 9. F -value as a function of frequency when an image intensifier and sinusoidal or Dirac pulse train excitation are used. The optimal angles according to Fig. 8 were used in the calculations.

$$\bar{\tau} = \tan \bar{\alpha} = \frac{s_1 \cos \phi_2 - s_2 \cos \phi_1 - s_3 (\cos \phi_2 - \cos \phi_1)}{s_1 \sin \phi_2 - s_2 \sin \phi_1 - s_3 (\sin \phi_2 - \sin \phi_1)}. \quad (56)$$

The expressions for $E\{U\}$ and $E\{V\}$ are the same as those in Eqs. (39) and (40). We get

$$D^2\{U\} = N[\cos^2 \phi_2 D^2\{X_1\} + \cos^2 \phi_1 D^2\{X_2\} + (\cos \phi_2 - \cos \phi_1)^2]. \quad (57)$$

We have

$$\begin{aligned} D^2\{X_i\} &= E\{X_i^2\} \\ &= 1 + 2 \operatorname{Im}[\exp(i\phi_i)q_{-1}] \\ &\quad + \frac{1}{2} \operatorname{Re}[1 - \exp(2i\phi_i)q_{-2}] \\ &= \frac{3}{2} + m \cos \alpha \cos(\phi_i + \alpha). \end{aligned} \quad (58)$$

Inserting Eq. (58) into Eq. (57), we will get $D^2\{U\}$. Replacing the cosines with sines, we get $D^2\{V\}$. We also have

$$E\{UV\} = N[\sin \phi_2 \cos \phi_2 D^2\{X_1\} + \sin \phi_1 \cos \phi_1 D^2\{X_2\} + (\cos \phi_2 - \cos \phi_1)(\sin \phi_2 - \sin \phi_1)]. \quad (59)$$

As with Dirac pulse excitation, the relative accuracy σ_τ/τ cannot be written as a function of $\Delta\phi = \phi_2 - \phi_1$. When ϕ_1 and ϕ_2 are varied, the ratio between the largest and smallest values of σ_τ/τ is approximately 4. We get $F_{\min} = 7.4$, attained for $\alpha = 35^\circ$, corresponding to $\tau = \omega\tau^* = 0.69$. This means that the optimum modulation frequency is $0.11/\tau^*$ (Fig. 9). For any α , the minimal F -value is attained for $\phi_1 + \alpha \approx 120^\circ$ and $\phi_2 + \alpha \approx -120^\circ$ (compare with Fig. 8).

E. Demodulation

The fluorescent light varies sinusoidally with an unknown phase angle ϕ_0 [compare with Eq. (34)]:

$$q(t) = \frac{1}{2\pi}[1 + m \cos \alpha \sin(t - \phi_0 - \alpha)]. \quad (60)$$

Here the modulation degree m of the excitation light is supposed to be known, and the parameter $\alpha = \arctan \tau$ is to be determined. The idea is to determine α from the degree of modulation $m \cos \alpha$ and not from the phase shift in $\sin(t - \phi_0 - \alpha)$. This is achieved by multiplying the signal by $1 + \sin(t + \phi_i)$ for three different phases ϕ_1 , ϕ_2 , and ϕ_3 , thus producing the measurements s_1 , s_2 , and s_3 . This can be done either with an image intensifier or with dc-biased lock-in amplifiers.

First, we use s_1 , s_2 , and s_3 to determine the unknown phase ϕ_0 . Then the obtained ϕ_0 is inserted in the equations with the aim of extracting the factor $m \cos \alpha$ of Eq. (60). This leads to calculating the following two complex determinants:

$$U = \det \begin{bmatrix} s_1 & \exp(i\phi_1) & 1 \\ s_2 & \exp(i\phi_2) & 1 \\ s_3 & \exp(i\phi_3) & 1 \end{bmatrix},$$

$$V = \det \begin{bmatrix} s_1 & \exp(-i\phi_1) & \exp(i\phi_1) \\ s_2 & \exp(-i\phi_2) & \exp(i\phi_2) \\ s_3 & \exp(-i\phi_3) & \exp(i\phi_3) \end{bmatrix}. \quad (61)$$

U and V are linear expressions in the observed s_i , and we want to calculate their expectations. As above, $E\{s_i\} = NE\{X_i\}$, and we have [compare with Eq. (54)]

$$\begin{aligned} E\{X_i\} &= 1 + \operatorname{Im}\{\exp[i(\phi_i + \phi_0)]q_{-1}\} \\ &= 1 + \frac{m \cos \alpha}{2} \cos(\phi_i + \phi_0 + \alpha). \end{aligned} \quad (62)$$

Inserting Eq. (62) in Eq. (61) and doing column operations on the determinants, we obtain

$$\begin{aligned} E\{U\} &= \frac{iNm \cos \alpha}{2} \exp[-i(\alpha + \phi_0)][\sin(\phi_3 - \phi_2) \\ &\quad + \sin(\phi_1 - \phi_3) + \sin(\phi_2 - \phi_1)], \end{aligned} \quad (63)$$

$$\begin{aligned} E\{V\} &= 2iN[\sin(\phi_3 - \phi_2) + \sin(\phi_1 - \phi_3) \\ &\quad + \sin(\phi_2 - \phi_1)]. \end{aligned} \quad (64)$$

We find that

$$\frac{|E\{U\}|}{|E\{V\}|} = \frac{m \cos \alpha}{4}. \quad (65)$$

As usual, the observed u and v are assumed to be estimates of $E\{U\}$ and $E\{V\}$, respectively. If the number $4|u|/(m|v|)$ obtained in a particular measurement is less than unity, it will be used as an estimate of $\cos \alpha$.

As is seen in Eqs. (64) and (65), the three phase angles ϕ_1 , ϕ_2 , and ϕ_3 contribute to $E\{U\}$ and $E\{V\}$ with the same real factor

$$\begin{aligned} \delta(\phi_1, \phi_2, \phi_3) &= \sin(\phi_3 - \phi_2) + \sin(\phi_1 - \phi_3) \\ &\quad + \sin(\phi_2 - \phi_1). \end{aligned} \quad (66)$$

Since $\delta(\phi_1, \phi_2, \phi_3)$ is cancelled in Eq. (65), this expression is independent of the three phases as long as $\delta(\phi_1, \phi_2, \phi_3) \neq 0$. If δ is small, $|u|/|v|$ is the ratio between small numbers and may suffer from discretization errors. A simple advice is to let the ϕ_i be 120° apart, which maximizes $|\delta|$.

The variances $D^2\{U\}$ and $D^2\{V\}$ can be calculated with formulas analogous to Eq. (57) by using Eq. (58), which is valid here. If the measurements are made with lock-in amplifiers, the three s_i will be observations of dependent random variables. Then a laborious trigonometric reduction of the expressions will result in

$$D^2\{V\} = (E\{V\})^2/N, \quad D^2\{U\} = \frac{1}{8}D^2\{V\}. \quad (67)$$

Demodulation

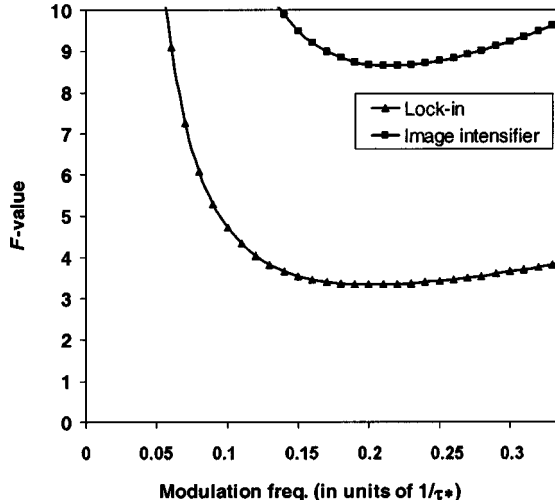


Fig. 10. F -value as a function of frequency with the use of demodulation for determining lifetime. Sinusoidal excitation was assumed in both cases.

We have found empirically that $\rho \approx (\cos \alpha)/\sqrt{2}$. Inserting these quantities in Eq. (6) and skipping powers of N^{-1} higher than unity, we get

$$\left(\frac{\sigma_{\cos \alpha}}{\cos \alpha} \right)^2 = \frac{1}{Nm^2 \cos^2 \alpha} [1 + \sin^2 \alpha + (1 - m)^2 \cos^2 \alpha]. \quad (68)$$

To get τ from the calculated $\cos \alpha$, we shall apply the formula

$$\tau = \tan \alpha = (\cos^{-2} \alpha - 1)^{1/2}. \quad (69)$$

For small errors (large N), we have approximately

$$\frac{\sigma_\tau}{\tau} = \left| \frac{d\tau}{d \cos \alpha} \right| \frac{\cos \alpha}{\tau} \frac{\sigma_{\cos \alpha}}{\cos \alpha} = \frac{1}{\sin^2 \alpha} \frac{\sigma_{\cos \alpha}}{\cos \alpha}. \quad (70)$$

We get

$$\begin{aligned} F &= \sqrt{N} \frac{\sigma_\tau}{\tau} \\ &= \frac{1}{m \cos \alpha \sin^2 \alpha} [1 + \sin^2 \alpha + (1 - m)^2 \cos^2 \alpha]^{1/2}. \end{aligned} \quad (71)$$

For the modulation $m = 1$, we get $F_{\min} = 3.33$, attained for $\cos \alpha = (\sqrt{5} - 1)/2$, corresponding to $\tau = 1.27$. The minimizing τ will increase toward $\sqrt{2}$ when the modulation tends to zero. With $\tau = \omega \tau^* = 1.27$, the minimizing modulation frequency will be $0.20/\tau^*$ (Fig. 10).

If an image intensifier is used for the detection, the s_i will be measured sequentially, so that they become independent. The first moments of $|U|$ and $|V|$ are still independent of the phase angles, but the second moments will depend on all the phase angles, even ϕ_0 . Here it is imperative to choose the ϕ_1 , ϕ_2 , and ϕ_3 120° apart. Otherwise, the correlation between $|U|$ and $|V|$ can become negative, and this will ruin the accuracy. We have failed to deduce theoretical expressions for the second moments in this case with independent s_i . With the ϕ_i 120° apart, we have run a sequence of Monte Carlo tests with different α and N and obtained the following estimates [compare with Eq. (67)]:

$$D^2\{U\} \approx (E\{V\})^2/(4N), \quad D^2\{V\} \approx (E\{V\})^2/(2N), \quad (72)$$

and $\rho \approx (\cos \alpha)/2$. With the modulation $m = 1$, the Monte Carlo tests give $F_{\min} = 8.64$ for $\tau = \omega \tau^* \approx 1.4$ (modulation frequency $0.22/\tau^*$) (Fig. 10).

3. MONTE CARLO SIMULATION

We have compared all our theoretical results with Monte Carlo simulations of the photon generation and measuring methods. The agreement is good. An example of

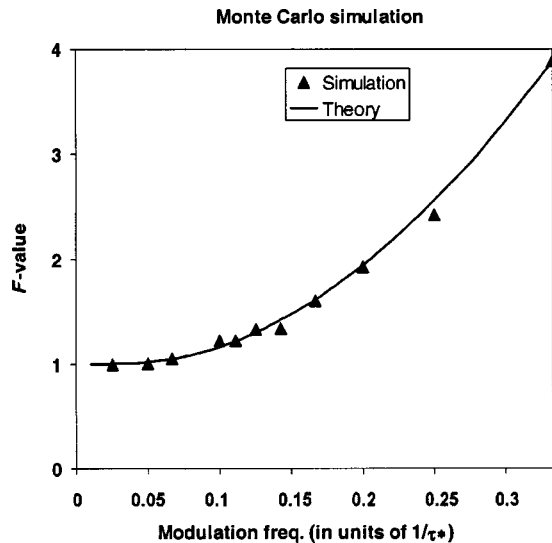


Fig. 11. Results from Monte Carlo simulation and the corresponding theoretical curve. The case shown is Dirac pulse excitation and lock-in detection.

this is given in Fig. 11. The simulations also give a few quantities of the demodulation technique that we could not deduce analytically.

Each period of the time axis is divided into intervals of length $\Delta t = 2\pi/M$, M large. For each interval, a pseudorandom number is used to determine whether a photon shall be generated or not, according to, e.g., the probability density $p(t)\Delta t$ of Eq. (8) (compare with Fig. 1). M is chosen sufficiently large that $p(t)\Delta t$ is less than 0.01 for all t in order to keep the probability of several photons per interval low. The resulting M ranges from 30,000 to several millions depending on τ , N , and the method.

When we simulate lock-in detection and a photon is generated in the interval $(t, t + \Delta t)$, the number $\sin(t + \phi_1)$ is added to s_1 , and analogously for the other amplifiers and detection methods. The estimate $\bar{\tau}$ is calculated according to an appropriate formula such as Eq. (13). This simulation of a measurement is repeated several (often 1000) times, and statistics of the obtained quantities are collected. In this way, we get estimates of $E\{\bar{\tau}\}$, $D^2\{\bar{\tau}\}$, $E\{U\}$, $E\{U^2\}$, F , and so on.

All simulations were carried out for measurements with $N = 240$ and $N = 2400$ photons per measurement, which are typical values in real applications. Various values of τ , modulation m , and phase angles ϕ_i were tested, all giving results in good agreement with the theory. A more detailed account of the simulations is given in Ref. 27.

4. CONCLUSIONS

We have shown that frequency-domain fluorescence lifetime imaging methods have the potential of using the available photons efficiently, provided that the recording parameters are selected correctly. In all cases, the parameter choice is governed by the lifetime of the fluorophore to be recorded. In reality, the lifetime will vary, often in an unpredictable way, across the specimen area (this is the information that we want to record!). Therefore it is not, in general, possible to use the optimum pa-

rameter choice for all parts of the recorded lifetime image. Based on an average expected lifetime, it should, however, be possible to make a good compromise.

An interesting result of the study is that the optimum modulation frequency of the illuminating light is rather low. In general, optimum performance is obtained at a frequency of approximately $0.1/\tau^*$. This means that for a typical fluorophore lifetime of, say, 3 ns, a frequency of approximately 30 MHz is optimal. The use of such a low frequency means that the bandwidth requirements for light source and electronics are moderate. As a consequence, the equipment will be less expensive.

We have also shown that the excitation waveform can be quite important and that sinusoids are not optimal. The best results are obtained with trains of Dirac pulses, but square waves with a duty cycle ≤ 0.2 also perform well. Even a square wave with a duty cycle of 0.5 is better than a sinusoid. The steep flanks of a square wave require a high modulation bandwidth. Therefore it is important to note that a strongly smoothed square wave can be used without losing much of the performance. For example, for $\tau^* = 3$ ns the use of smooth "Gauss-like" excitation pulses having a FWHM of 7 ns at a pulse-repetition frequency of 28 MHz will give an F -value of 1.55. Then the bandwidth requirement for the light source is only approximately 50 MHz. With sinusoidal excitation, the corresponding F -value is 3.77.

Some lock-in amplifiers can mix the input with either a sinusoid or a square wave. Our Monte Carlo tests show that it is better to combine a sinusoidal excitation with a sinusoidal lock-in than with a square-wave lock-in. A square wave for both excitation and lock-in is not a good combination because it gives no stable way for estimating τ .

Address correspondence to Johan Philip at the location on the title page or by e-mail, johanph@math.kth.se.

REFERENCES

- C. G. Morgan, A. C. Mitchell, and J. G. Murray, "Nanosecond time-resolved fluorescence microscopy: principles and practice," *Trans. R. Microsc. Soc.* **1**, 463–466 (1990).
- E. P. Buurman, R. Sanders, A. Draaijer, H. C. Gerritsen, J. J. F. van Veen, P. M. Houpt, and Y. K. Levine, "Fluorescence lifetime imaging using a confocal laser scanning microscope," *Scanning* **14**, 155–159 (1992).
- D. W. Piston, D. R. Sandison, and W. W. Webb, "Time-resolved fluorescence imaging and background rejection by two-photon excitation in laser scanning microscopy," in *Time-Resolved Laser Spectroscopy in Biochemistry III*, J. R. Lakowicz, ed., Proc. SPIE **1640**, 379–389 (1992).
- T. W. J. Gadella, T. M. Jovin, and R. M. Clegg, "Fluorescence lifetime imaging microscopy (FLIM): spatial resolution of microstructures on the nanosecond timescale," *Bioophys. Chem.* **48**, 221–239 (1993).
- R. Müller, C. Zander, M. Sauer, M. Deimel, D.-S. Ko, S. Siebert, J. Arden-Jacob, G. Deltau, N. J. Marx, K. H. Drexhage, and J. Wolfrum, "Time-resolved identification of single molecules in solution with a pulsed semiconductor diode laser," *Chem. Phys. Lett.* **262**, 716–722 (1996).
- A. H. Buist, M. Müller, E. J. Gijsbers, G. J. Brakenhoff, T. S. Sosnowski, T. B. Norris, and J. Squier, "Double-pulse fluorescence lifetime measurements," *J. Microsc. (Oxford)* **186**, 212–220 (1997).
- M. Sauer, J. Arden-Jacob, K. H. Drexhage, F. Göbel, U. Lieberwirth, K. Mühlberger, R. Müller, J. Wolfrum, and C.

- Zander, "Time-resolved identification of individual mononucleotide molecules in aqueous solution with pulsed semiconductor lasers," *Bioimaging* **6**, 14–24 (1998).
8. J. Sytsma, J. M. Vroom, C. J. de Grauw, and H. C. Gerritsen, "Time-gated fluorescence lifetime imaging and micro-volume spectroscopy using two-photon excitation," *J. Microsc. (Oxford)* **191**, 39–51 (1998).
 9. C. J. de Grauw and H. C. Gerritsen, "Multiple time-gate module for fluorescence lifetime imaging," *Appl. Spectrosc.* **55**, 670–678 (2001).
 10. T. Oida, Y. Sako, and A. Kusumi, "Fluorescence lifetime imaging microscopy (flimscopy)," *Biophys. J.* **64**, 676–685 (1993).
 11. C. J. R. van der Oord, H. C. Gerritsen, F. F. G. Rommerts, D. A. Shaw, I. H. Munro, and Y. K. Levine, "Micro-volume time-resolved fluorescence spectroscopy using a confocal synchrotron radiation microscope," *Appl. Spectrosc.* **49**, 1469–1473 (1995).
 12. P. T. C. So, T. French, W. M. Yu, K. M. Berland, C. Y. Dong, and E. Gratton, "Time-resolved fluorescence microscopy using two-photon excitation," *Bioimaging* **3**, 49–63 (1995).
 13. A. Draaijer, R. Sanders, and H. C. Gerritsen, "Fluorescence lifetime imaging, a new tool in confocal microscopy," in *Handbook of Biological Confocal Microscopy*, J. Pawley, ed. (Plenum, New York, 1995), pp. 491–505.
 14. K. König, P. T. C. So, W. W. Mantulin, B. J. Tromberg, and E. Gratton, "Two-photon excited lifetime imaging of auto-fluorescence in cells during UVA and NIR photostress," *J. Microsc. (Oxford)* **183**, 197–204 (1996).
 15. H. Brismar and B. Ulfhake, "Fluorescence lifetime measurements in confocal microscopy of neurons labeled with multiple fluorophores," *Nat. Biotechnol.* **15**, 373–377 (1997).
 16. T. French, P. T. C. So, D. J. Weaver, T. Coelho-Sampaio, and E. Gratton, "Two-photon fluorescence lifetime imaging microscopy of macrophage-mediated antigen processing," *J. Microsc. (Oxford)* **185**, 339–353 (1997).
 17. A. Squire and P. I. H. Bastiaens, "Three dimensional image restoration in fluorescence lifetime imaging microscopy," *J. Microsc. (Oxford)* **193**, 36–49 (1999).
 18. K. Carlsson, A. Liljeborg, R. M. Andersson, and H. Brismar, "Confocal pH imaging of microscopic specimens using fluorescence lifetimes and phase fluorometry: influence of parameter choice on system performance," *J. Microsc. (Oxford)* **199**, 106–114 (2000).
 19. J. R. Lakowicz and H. Szmacinski, "Fluorescence lifetime-based sensing of pH, Ca^{+2} , K^+ and glucose," *Sens. Actuators B* **11**, 133–143 (1993).
 20. G. Krishnamoorthy and A. Srivastava, "Intracellular dynamics seen through time-resolved fluorescence microscopy," *Curr. Sci.* **72**, 835–845 (1997).
 21. R. D. Spencer and G. Weber, "Measurements of subnanosecond fluorescence lifetimes with a cross-correlation phase fluorometer," *Ann. N. Y. Acad. Sci.* **158**, 361–376 (1969).
 22. D. V. O'Connor and D. Phillips, *Time-Correlated Single Photon Counting* (Academic, New York, 1984).
 23. M. Köllner and J. Wolfrum, "How many photons are necessary for fluorescence lifetime measurements?" *Chem. Phys. Lett.* **200**, 199–204 (1992).
 24. R. M. Ballew and J. N. Demas, "An error analysis of the rapid lifetime determination method for the evaluation of single exponential decays," *Anal. Chem.* **61**, 30–33 (1989).
 25. E. Gaviola, "Ein Fluorometer. Apparat zur Messung von Fluoreszenzabklingzeiten," *Z. Phys.* **42**, 853–861 (1927).
 26. K. Carlsson and A. Liljeborg, "Simultaneous confocal lifetime imaging of multiple fluorophores using the intensity-modulated multiple-wavelength scanning (IMS) technique," *J. Microsc. (Oxford)* **191**, 119–127 (1998).
 27. K. Carlsson and J. Philip, "Theoretical investigation of the signal-to-noise ratio for different fluorescence lifetime imaging techniques," in *Optical Diagnostics of Living Cells V*, D. L. Farkas and R. C. Leif, eds., Proc. SPIE **4622**, 70–78 (2002).
 28. K. Carlsson and A. Liljeborg, "Confocal fluorescence microscopy using spectral and lifetime information to simultaneously record four fluorophores with high channel separation," *J. Microsc. (Oxford)* **185**, 37–46 (1997).